Anal. Bioanal. Electrochem., Vol. 11, No. 2, 2019, 178-188

Analytical & Bioanalytical Electrochemistry

www.abechem.com

Full Paper

Electrochemical Synthesis of Magnetite Nanoparticles through Base Electrogeneration Strategy and their Doping with Nickel(II) Cations and Surface Capping with Mono-, Di- and Polysaccharides

Ali Ahmadi[1] and Kazem Mohammadzadeh[2,*]

[1]*Materials and Nuclear Research School, Nuclear Science and Technology Research Institute (NSTRI), P.O. Box 14395-834, Tehran, Iran*

[2] *School of Chemical Engineering, Iran University of Science and Technology, Narmak 16846-13114, Tehran, Iran*

*Corresponding Author,

E-Mail: K_mohammadzadeh@chemeng.iust.ac.ir

Received: 3 November 2018 / Received in revised form: 25 December 2018 / Accepted: 12 January 2019 / Published online: 28 February 2019

Abstract- In this paper, magnetic iron oxide nanoparticles capped with glucose/sucrose/starch have been synthesized though a simple and easy electrochemical method. In this method, OH^- anions were produced *via* galvanostatic cathodic current on the cathode surface, and then reacted with metal cations (i.e. Fe^{2+}, Fe^{3+} and Ni^{2+}) to form Ni-doped Fe_3O_4 deposit. At the same electrochemical conditions, saccharides capped Ni-doped iron oxides were also synthesized from saccharide-added electrolyte. The prepared samples were specified using FE-SEM, XRD, VSM, FT-IR and thermal gravimetric analyses. The FT-IR, XRD and FE-SEM data approved the formation of Ni-doped Fe_3O_4 particles with size of 30 nm. In the TG profiles, the sharp weight loss (~15.5%wt.) at the temperatures of 150-300 ^oC proved the capping of iron oxide surfaces by saccharide layer. The measured magnetic data by VSM analyses indicated that the prepared samples exhibit high saturation magnetization and low remanence at the applied external fields, and have proper superparamagnetic characters.

Keywords- Electrochemical Synthesis, Iron Oxide, Nanoparticles, Surface capping, Biomedical

1. INTRODUCTION

Metal oxides with particle morphology and size of less than 100 nm have great potential interest for use in various applications like as biomedicine, energy storage, catalyst, and gas sensing, biosensor systems, which is due to their low cost, high surface area and facile preparation [1-12].

Among metal oxides, iron oxides (especially magnetite) have been intensively studied, and it has proven that nanoparticles of Fe_3O_4 are valuable candidates for use in magnetic hyperthermia [13-18], drug carrier [19-25], charge storage [26-32], magnetic resonance imaging (MRI) [33-36], etc.

Up now, Fe_3O_4 nanoparticles have been fabricated through various methods including thermal decomposition, solvothermal, co-precipitation, sol-gel, microemulsion, hydrothermal and microwave assisted synthesis [37,38]. Besides these synthetic platforms, electrochemical strategy has been also described to be a facile and simple technique for production of Fe_3O_4 nanoparticles [39-42]. It was also proven that nanoparticles of various metal oxides and hydroxides (MOHs) could be simply produced through two-electrode deposition system [43-50]. However, Fe_3O_4 stability after production is a prerequisite for the above mentioned applications. Naked nanoparticles tend to adhere together and form bigger spheres/agglomerates because of high surface area-to-volume ratio [51]. Hence, surface capping is needed to give them colloidal stability and hinder agglomeration. In fact, Fe_3O_4 nanoparticles are generally aggregated in absence of proper surface coat layer. To solve these defects, surface capping of Fe_3O_4 nanoparticles should be designed and carried out during/or after production procedure [52,53]. Notably, surface capping has mentioned as a key procedure to overcome the limitations associated with the Fe_3O_4 nanoparticles applications in nano-/bio-medicine. The surface charge, reactivity, functionality and, size of Fe_3O_4 nanoparticles could be manipulated through surface capping strategy, which remit nanoparticles to be more chemically stable and suitable for *in vivo* uses [54-56]. In this regards, surface of Fe_3O_4 nanoparticles has been capped with different agents like as PEG, PVP, PVA, chitosan, dextran, and biomolecules. And their biological and physico-chemical properties have been investigated [57-65].

Herein, we applied electrochemical base (OH^-) generation strategy for the producing Fe_3O_4 nanoparticles and their simultaneously doping and surface capping. This strategy has been previously used to fabricate metal ion doped Fe_3O_4 nanoparticles [66-71], however, in-situ Ni^{2+} doping and polysaccharides capping of Fe_3O_4 nanoparticles has not been reported. Galvanostatic mode in a two-electrode configuration was selected for preparing the Fe_3O_4 nanoparticles. The nickel cations were used as dopant, and glucose, sucrose and starch (as mono-, di- and polysaccharides, respectively) applied to cover the surface of produced Fe_3O_4 nanoparticles. The fabricated samples were named as IO-1, IO-2 and IO-3, respectively, for the capped nanoparticles with glucose, sucrose and starch saccharides. The resulting samples were

analyzed by FE-SEM, XRD, DSC-TGA, VSM, and FT-IR techniques to determine their physic-chemical and magnetic properties.

2. EXPERIMENTAL PROCEDURE

2.1. Materials

The chemical reagents including iron(II) chloride hexahydrate, iron(III) nitrate nonahydrate, nickel nitrate hexahydrate, ethanol (96%), starch, glucose and sucrose were purchased from Sigma-Aldrich chemical company.

2.2. Synthesis of iron oxide samples

All the electrodeposition experiments were designed based on the cathodic electrodeposition via base generation strategy. A simple aqueous electrolyte containing 3 mM iron(II) chloride, 1mM nickel chloride, 8 mM iron(III) nitrate and 1mM saccharide (sucrose or starch or glucose) was used in the synthesis process. The electrochemical cell was two stainless steel sheet immerged into the electrode and connected to the external power supply by Cu wires. The optimum applied experimental values were i=10 mA cm^{-2}, t=25min and pH=6.2. After synthesis, the electrode was removed from the bath solution, and the deposited black film was separated from the electrode surface. Then this powder was washed several times with ethanol and heated at 70 ^{o}C for 2h in vacuum oven. The final powders were used in analyses tests.

2.3. Sample characterization

The crystalline nature and phase information of the prepared IOs were obtained by X-ray diffraction (XRD), using a Phillips PW-1800 diffractometer. The patterns were provided by using Cu-Kα radiation (λ=1.5406Å) in the zone of 10^{o}<2theta<80^{o} with steps of 0.015 and acquisition time of 2s/step. The surface capping was confirmed by a Bruker Vector 22 Fourier transform infrared (FT-IR) spectroscope. The IR spectra of sample were collected in the frequency range of 4000–400 cm^{-1} with resolution of 1.5 cm^{-1}. The surface morphology observations of the samples were carried out by field-emission scanning electron microscopy (FE-SEM, Mira 3-XMU with accelerating voltage of 100 kV), and FE-SEM images were provided. Thermal behavior of IO samples was analyzed via PerkinElmer Instruments model, STA 1500 equipment at a heating rate of 5 ^{o}C/min in the temperature zone of 25-500 ^{o}C under N2 atmosphere, and DSC-TG profiles were obtained. The magnetization profiles were collected on Vibrating Sample Magnetometers (VSM, model Lakeshore 7410) at RT in the range of −20000 to 20000 Oe.

3. RESULTS AND DISCUSSION

3.1. Morphological characterization

Surface observations of IO samples provided by FE-SEM are presented in Fig. 1. For the IO samples, i.e. IO-1, IO-2 and IO-3, particle-shape morphology is seen in the FE-SEM images (Figs. 1a-c). Notably, the observed particles are rather agglomerated in nature, and their average size was calculated to be 30 nm.

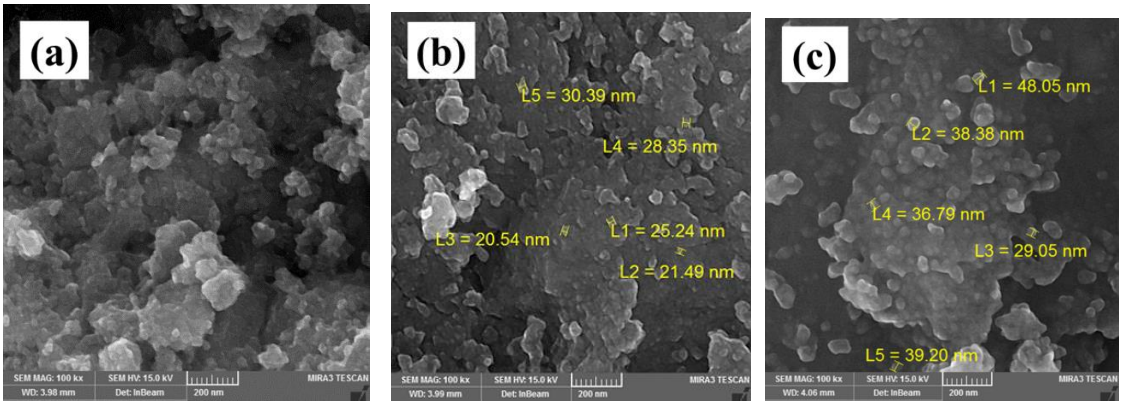

Fig. 1. FE-SEM images of the prepared (a) IO-1, (b) IO-2, and (c) IO-3 nano-particles

3.2. XRD

The powder X-ray diffraction (i.e. XRD) patterns of the electro-deposited IO-1, IO-2 and IO-3 samples are provided in Fig. 2. For all sample, well-defined diffractions of (111), (220), (311), (400), (422), (511), (440), (620) and (533) are present in Fig. 2.

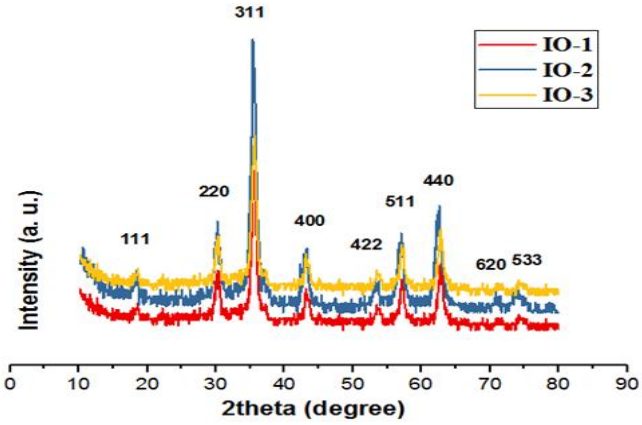

Fig. 2. XRD patterns of the fabricated iron oxide samples

These planes are well-fitted with those mentioned for Fe_3O_4 crystal phase of iron oxide (JCPDS No.85-1436) [69-72]. The average crystallite sizes of IO-1, IO-2 and IO-3 sample was assessed through Debye Scherrer relation, i.e. $D= k\lambda/\beta\cos\theta$, where β is the full width of (311)

plane at its half maximum (FWHM), λ is the X-ray beam wavelength (λ_{Cu}=1.54Å), θ is the Bragg angle for the actual peak and k is a shape function, where k=0.9 was used [69]. It was found that the average crystallite sizes were 13.3, 14.54 and 15.72 nm for IO-1, IO-2 and IO-3, respectively.

3.3. FT-IR

FTIR analysis was implemented to get information about chemical composition and surface chemistry of the prepared IO samples. Fig. 2 shows the IR spectra of the electrodeposited iron oxide powders. Notably, for better presenting the IR bands located at low wavenumber range (i.e. 400-700 cm^{-1}), this zone has magnified and provided in the inset of Fig. 2. For all samples, four definite IR band are observed at the wavenumber range of 400-700 cm^{-1}, which are related to the vibrations of Fe-O-Fe/or Fe-O-Ni chemical bonds. Two IR adsorption at 571 cm^{-1} and 668 cm^{-1} are arise from splitting the ν_1 band of the Fe—O bond, and the peaks at 439 cm^{-1} and 465 cm^{-1} are also resulted from the ν_2 bands of the Fe—O/Ni-O bonds [60,69,72-75]. These IR data proved the Ni doped and magnetite phase for the prepared samples.

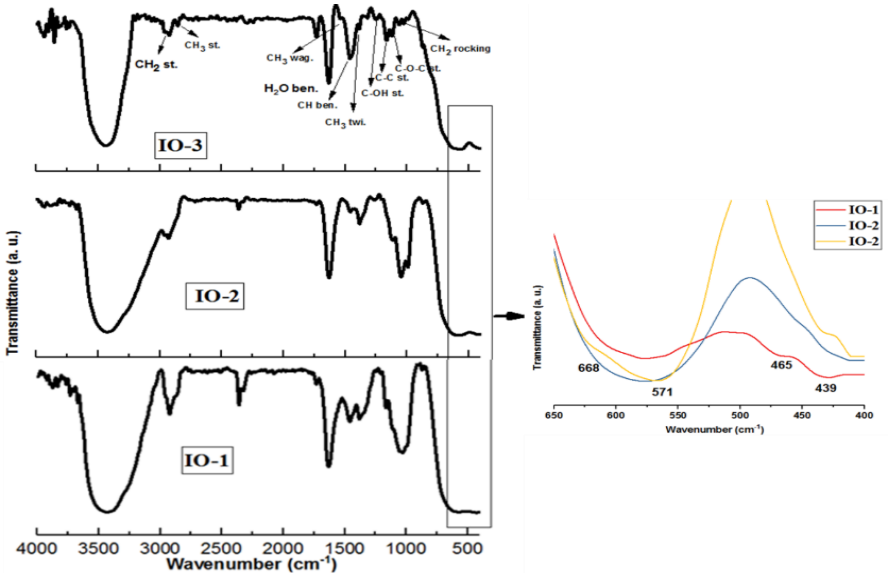

Fig. 3. IR spectra of the electrochemically deposited IO-1, IO-2 and IO-3 samples

Furthermore, several IR bands are observed for all samples, which are located at about identical wavenumbers (Fig. 2). These IR peaks are due to the follows chemical bonds [73-80]: oxygen-hydrogen bond stretching of –OH groups at 3400–3500 cm^{-1} [73,74], $\nu_{bending}$ of physically adsorbed H_2O and 1630-1640 cm^{-1}, $\nu_{asymmetric}$ stretching of CH_2 at 2930-2940 cm^{-1} [75], $\nu_{wagging}$ of CH_2 at 1380-1385 cm^{-1} [76,78], $\nu_{symmetric}$ stretching of CH_2 at 2875-2890 cm^{-1} [78,79], $\nu_{rocking}$ of CH_2 at 880-885 cm^{-1} [74,80], $\nu_{scissoring}$ of CH_2 at 1450-1460 cm^{-1}, $\nu_{twisting}$ of CH_2 at 1280-1285 cm^{-1}, $\nu_{bending}$ of C-H at 1310-1320 cm^{-1} [79,80], $\nu_{stretching}$ of C-OH at 1240-

1250 cm^{-1} [80,81] and $\nu_{stretching}$ of carbon-oxygen bond located at the glucose ring at 1010-1020 cm^{-1} [73,82]. These IR bands showed the presence of same chemical bonds/groups on the composition of the prepared samples, including of carbon-carbon bond, carbon-hydrogen bond, carbon-oxygen bond, C-OH bond, and $–CH_2$ group. Based on these findings, the saccharide capped layer onto deposited iron oxide particles is confirmed.

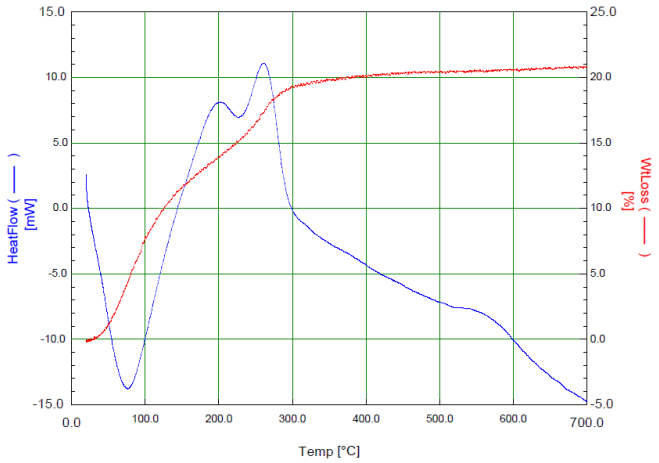

Fig. 4. DSC-TG profiles of the sucrose coated iron oxide NPs i.e. IO-2 sample

3.4. Thermogravimetric (DCS-TG) analyses

To determine the surface capping of the oxide samples by saccharides, the thermal stability of iron oxide nanoparticles was done through thermogravimetric technique. In this regard, IO-2 powder was heated at the special heating rate of 5°/min, and its weight change was measured. The obtained data were plotted as DSC-TGA profiles in Fig. 4. In this graph, the changes in low temperatures of 25-150 °C are related to the removal of adsorbed water onto the iron oxide [60,63]. For this step, an endothermic peak is observed on DSC profile, and a small weight loss of 5% is also occurred on the TG curve. After this step, between the temperatures of 150-300 °C, a two successive endothermic peaks are appeared on the DSC curve (as seen in Fig. 4), which can be assigned to the decomposition of saccharide chain around the surface of iron oxide particles and its removal from the IO-2 powder [73,82]. The weight change of IO-2 sample in this temperature range was estimated to be 14.95% (as seen in TG curve). This change is completely approved the sucrose molecules attached onto the iron oxide particles. After this change, magnetite oxidation into the hematite and/or maghemite structure is observed at the temperatures of 150-300 °C, where 1.1% weight loss was occurred on the TG profile.

3.5. Magnetic behavior

To evaluate the magnetization performance of the electro-deposited iron oxide samples, their behavior in the presence/and absence of external field was determined through measuring the magnetization values *vs.* applied field. The obtained hysteresis profiles for the prepared

iron oxides are shown in Fig. 5. Reversible form of the VSM curves (in Fig. 5) and absence of any hysteresis loop specified that all samples have superparamagnetic behavior. The saturation magnetizations (*Ms*) values of 62.73 emu g^{-1}, 59.27 emu g^{-1} and 56.85 emu g^{-1} for IO-1, IO-2 and IO-3 samples, respectively. These relative high values *Ms* clearly indicated the superparamagnetic performance of the samples at the presence of external field. However, these *Ms* values are smaller than those reported for bulk or naked Fe_3O_4 NPs (i.e. 98-102 emu g^{-1}[79-81]). Furthermore, the other measured magnetic values were:

- *Positive Hci=-5.95G, Mr=0.29 emu g^{-1}, negative Hci=-12.5G, negative Mr=0.17 emu g^{-1}, positive Mr=0.41 emu g^{-1}, and Hci=9.04G* for glucose capped iron oxide NPs (i.e. IO-1 sample),
- *Positive Hci=-5.83G, negative Hci=-13.4G, negative Mr=0.21 emu g^{-1}, Mr=0.36 emu g^{-1}, positive Mr=0.51 emu g^{-1}, and Hci=9.61G* for sucrose capped iron oxide NPs (IO-2 sample), and
- *Mr*=0.23 emu g^{-1}, *Positive Hci=-1.5G, negative Mr*=0.08 emu g^{-1}, *positive Mr*=0.38 emu g^{-1}, *negative Hci=-9.5G,* and *Hci*=5.5G for starch capped iron oxide NPs (IO-3 sample).

The observed low *Mr* and *Hci* values indicate that the prepared samples exhibited low remanence and coercivity when applied field is cut off, and have suitable superparamagnetic behavior.

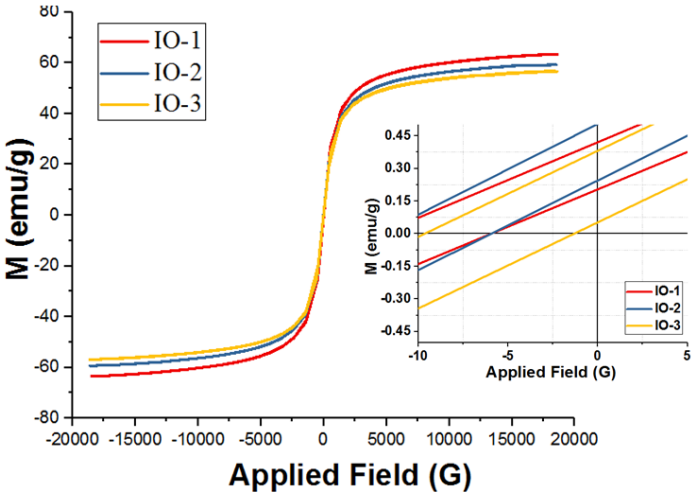

Fig. 5. Magnetization curves for the prepared IO-1, IO-2 and IO-3 samples

4. CONCLUSION

In summary, nanoparticles of magnetite phase of iron oxide were electro-synthesized *via* cathodic electrodeposition method. The analyses results confirmed that *in-situ* surface capping and metal-ion doping of Fe_3O_4 nanoparticles can be simultaneously achieved *via* galvanostatic cathodic electrodeposition. The prepared Ni-doped iron oxides exhibited superparamagnetic character at room temperature with reduced *Ms* compared to bulk magnetite. In addition, the

prepared particles possess acceptable high saturation magnetization, low remanence and negligible coercivity. It was also confirmed that the prepared saccharides-capped, Ni-doped iron oxide particles have all the physic-chemical and magnetic parameters for bio-medicinal uses.

REFERENCES

[1] P. Falcaro, R. Ricco, A. Yazdi, I. Imaz, S. Furukw, D. Maspoch, R. Ameloot, J. D. Evans, and C. J. Doonan, Coor. Chem. Rev. 307 (2016) 237.

[2] M. Rahimi-Nasrabadi, S. M. Pourmortazavi, M. Aghazadeh, M. R. Ganjali, M. Sadeghpour Karimi, and P. Novrouzi, J. Mater. Sci.: Mater. Electron. 28 (2017) 5574.

[3] D. Lisjaka, and A. Mertelj, Prog. Mater. Sci. 95 (2018) 286.

[4] H. M. Shiri, and A. Ehsani, Bull. Chem. Soc. Japan 89 (2016) 1201.

[5] M. Rahimi-Nasrabadi, S. M. Pourmortazavi, M. Aghazadeh, M. R. Ganjali, M. Sadeghpour Karimi, and P. Norouzi, J. Mater. Sci.: Mater. Electron. 28 (2017) 9478.

[6] K. Simeonidis, S. Mourdikoudis, E. Kaprara, M. Mitrakas, and L. Polavarapu, Environ. Sci.: Water Res. Technol. 2 (2016) 43.

[7] M. Rahimi-Nasrabadi, S.M. Pourmortazavi, M. Aghazadeh, M. R. Ganjali, M. Karimi, and P. Novrouzi. J. Mater. Sci.: Mater. Electron. 28 (2017) 3780.

[8] W. Lin, Chem. Rev. 115 (2015) 1040.

[9] M. Rahimi-Nasrabadis, S. M. Pourmortazavi, M. Aghazadeh, M. R. Anjali, M. Sadeghpour Karimi, and P. Norouzi J. Mater. Sci.: Mater. Electron. 28 (2017) 7600.

[10] M. Rahimi-Nasrabadi, S. M. Pourmortazavi, M. Sadeghpour Karimi, M. Aghazadeh, M. R. Ganjali, and P. Norouzi, J. Mater. Sci.: Mater. Electron. 28 (2017) 15224.

[11] M. Rahimi-Nasrabadi, S. M. Pourmortazavi, M. Sadeghpour Karimi, M. Aghazadeh, M. R. Ganjali, and P. Norouzi, J. Mater. Sci.: Mater. Electron. 28 (2017) 13267.

[12] H. M. Shiri, A. Ehsani, and M. J. Khales, J. Colloid Interface Sci. 505 (2017) 940.

[13] N. Griffete, J. Fresnais, A. Espinosa, D. Taverna, and C. Wilhelm, ACS Appl. Nano Mater. 1 (2018) 547.

[14] G. Kandasamy, A. Sudame, P. Bhati, A. Chakrabarty, S. N. Kale, and D. Maity, J. Colloid Interface Sci. 514 (2018) 534.

[15] C. Yadel, and J. Fresnais, Appl. Sci. 8 (2018) 1241.

[16] G. Kandasamy, A. Sudame, T. Luthra, K. Saini, and D. Maity, ACS Omega 3 (2018) 3991.

[17] M. Rahimi-Nasrabadi, S. M. Pourmortazavi, M. Sadeghpour Karimi, M. Aghazadeh, M. R. Ganjali, and P. Norouzi, J. Mater. Sci. Mater. Electron. 28 (2017) 6399.

[18] D. Chang, M. Lim, J. A. C. M. Goos, R. Qiao, Y. Y. Ng, F. M. Mansfeld, M. Jackson, T. P. Davis, and M. Kavallaris, Front. Pharmacol. 9 (2018) 831.

[19] R. Juneja, and I. Roy, Int. J. Nanomed. 13 (2018) 7.

[20] K. El-Boubbou, Nanomed. 13 (2018) 929.
[21] K. Kansara, P. Patel, R. K. Shukla, A. Pandya, R. Shanker, A. Kumar, and A. Dhawan, Int. J. Nanomed. 13 (2018) 79.
[22] S. Liang, Y. Wang, J. Yu, C. Zhang, J. Xia, 9.and D. Yin, J. Mater. Sci. Mater. Med. 18 (2007) 2297.
[23] O. A. Inozemtseva, S. V. German, N. A. Navolokin, A. B. Bucharskaya, G. N. Maslyakova, and D. A. Gorin, Nanotechnol. Biosensors Adv. Nanomater. (2018) 175.
[24] H. Nosrati, N. Sefidi, A. Sharafi, H. Danafar, and H. Kheiri Manjili, Bioorg. Chem. 76 (2018) 501.
[25] S. Kralj, T. Potrc, P. Kocbek, S. Marchesan, and D. Makovec, Curr. Med. Chem. 24 (2017) 454.
[26] M. Aghazadeh, I. Karimzadeh, and M. R. Ganjali, Mater. Lett. 209 (2017) 450.
[27] M. Aghazadeh, I. Karimzadeh, and M. R. Ganjali, J. Mater. Sci.: Mater. Electron. 28 (2017) 13532.
[28] M. Aghazadeh, and M. R. Ganjali, J. Mater. Sci. 53 (2018) 295.
[29] S. M. Pourmortazavi, M. Rahimi-Nasrabadi, M. Aghazadeh, M. R. Ganjali, M. Sadeghpour Karimi, and P. Norouzi, J. Electronic Mater. 46 (2017) 4627.
[30] M. Aghazadeh, and M. R. Ganjali, Ceram. Int. 44 (2018) 520.
[31] M. Aghazadeh, I. Karimzadeh, M. R. Ganjali, and A. Behzad, J. Mater. Sci.: Mater. Electron. 28 (2017) 18121.
[32] M. Aghazadeh, and M.R. Ganjali, J. Mater. Sci.: Mater. Electron. 29 (2018) 2291.
[33] F. Li, Z. Liang, J. Liu, J. Sun, X. Hu, M. Zhao, J. Liu, R. Bai, D. Kim, X. Sun, T. Hyeon, and D. Ling, Nano Lett. (2019) doi:10.1021/acs.nanolett.8b04411.
[34] M. Aghazadeh, and S. Dalvand, J. Electrochem. Soc. 161 (2014) D18.
[35] B. Mues, E. M. Buhl, T. Schmitz-Rode, and I. Slabu, J. Magn. Magn. Mater. 471 (2019) 432.
[36] N. Kang, D. Xu, Y. Han, X. Lv, Z. Chen, T. Zhou, L. Rena, and X. Zhou, Mater. Sci. Engin. C 98 (2019) 545.
[37] G. S. Demirera, A. C. Okur, and S. Kizilel, J. Mater. Chem. B 3 (2015) 7831.
[38] L. H. Reddy, J. L. Arias, J. Nicolas, and P. Couvreur, Chem. Rev. 112 (2012) 5818.
[39] M. Aghazadeh, Mater. Lett. 211 (2018) 225.
[40] M. Aghazadeh, I. Karimzadeh, and M. R. Ganjali, J. Mater. Sci.: Mater. Electron. 28 (2017) 19061.
[41] M. Aghazadeh, I. Karimzadeh, and M. R. Ganjali, Mater. Lett. 228 (2018) 137.
[42] M. Aghazadeh, I. Karimzadeh, and M. R. Ganjali, J. Electronic Mater. 47 (2018) 3026.
[43] M. Aghazadeh, M. G. Maragheh, M. R. Ganjali, and P. Norouzi, Inorg. Nano-Metal Chem. 27 (2017) 1085.
[44] M. Aghazadeh, J. Mater. Sci.: Mater. Electron. 28 (2016) 3108.

[45] M. Aghazadeh, R. Ahmadi, D. Gharailou, M. R. Ganjali, and P. Norouzi, J. Mater. Sci.: Mater. Electron. 27 (2016) 8623.
[46] M. Aghazadeh, A. A. M. Barmi, and M. Hosseinifard, Mater. Lett. 73 (2012) 28.
[47] M. Aghazadeh, M. Ghaemi, A. N. Golikand, and A. Ahmadi, Mater. Lett. 65 (2011) 2545.
[48] M. Aghazadeh, A. A. M. Barmi, H. M. Shiri, and S. Sedaghat, Ceram. Int. 39 (2013) 1045.
[49] M. Aghazadeh, M. G. Maragheh, M. R. Ganjali, and P. Norouzi, RSC Adv. 6 (2016) 10442.
[50] M. Aghazadeh, and I. Karimzadeh, Mater. Res. Express 4 (2017) 105505.
[51] R. Atchudan, B. G. Cha, N. Lone, J. Kim, and J. Joo, Korean J. Chem. Engin. 36 (2019 157.
[52] M. B. Silva Assis, I. H. S. Werneck, and G. N. Moraes, Mater. Res. Express 6 (2019) 045064.
[53] N. K. Katiyar, K. Biswas, C. S. Tiwary, L. D. Machado, and R. K. Gupta, Langmuir (2019) doi:10.1021/acs.langmuir.8b03401.
[54] M. Akbar, E. Cagli, and I. Erel-Göktepe, Macromol. Chem. Phys. (2019) doi.org/10.1002/macp.201800422.
[55] A. Tomitaka, A. Kaushik, B. D. Kevadiya, I. Mukadam, H. E. Gendelman, K. Khalili, G. Liu, and M. Nair, Drug Discovery Today (2019) doi.org/10.1016/j.drudis.2019.01.006.
[56] T. N. Britos, C. E. Castro, B. M. Bertassoli, G. Petri, F. L. A. Fonseca, F. F. Ferreir, and P. S. Haddad, Mater. Sci. Engin. C 99 (2019) 171.
[57] I. Karimzadeh, H. Rezagolipour Dizaji, and M. Aghazadeh, Mater. Res. Express. 3 (2016) 095022.
[58] I. Karimzadeh, M. Aghazadeh, M. R. Ganjali, and T. Dourudi, Curr. Nanosci. 13 (2017) 167.
[59] I. Karimzadeh, M. Aghazadeh, M. R. Ganjali, P. Norouzi, S. Shirvani-Arani, T. Doroudi, P. H. Kolivand, S. A. Marashi, and D. Gharailou, Mater. Lett. 179 (2016) 5.
[60] M. Aghazadeh, and I. Karimzadeh, Curr. Nanosci. 14 (2018) 42.
[61] Q. Zhang, Q. Liu, M. Du, A. Vermorken, Y. Cui, L. Zhang, L. Guo, L. Ma, and M. Chen, J. Magn. Magn. Mater. (2019) doi:10.1016/j.jmmm.2019.01.021.
[62] P. Norouzi, and M. Rezapour, Anal. Bioanal. Electrochem. 10 (2018) 1181.
[63] I. Karimzadeh, M. Aghazadeh, T. Doroudi, M. R. Ganjali, P. H. Kolivand, and D. Gharailou, Curr. Nanosci. 13 (2017) 274.
[64] M. Aghazadeh, and M. R. Ganjali, J. Mater. Sci.: Mater Electron. 28 (2017) 8144.
[65] M. Aghazadeh, J. Mater. Sci.: Mater. Electron. 28 (2017) 18755.
[66] M. Aghazadeh, I. Karimzadeh, and M. R. Ganjali, Phys. Status Solidi A 214 (2017) 1700365.

[67] M. Aghazadeh, M. Ghannadi Maragheh, and P. Norouzi, Int. J. Electrochem. Sci. 13 (2018) 1355.
[68] M. Aghazadeh, I. Karimzadeh, M. R. Ganjali, and M. Ghannadi Maragheh, J. Mater. Sci.: Mater. Electron. 29 (2018) 5163.
[69] M. Aghazadeh, and M. R. Ganjali, J. Mater. Sci.: Mater. Electron. 29 (2018) 4981.
[70] M. Aghazadeh, I. Karimzadeh, M. Ghannadi Maragheh, and M. R. Ganjali, Mater. Res. 21 (2018) e20180094.
[71] M. Aghazadeh, I. Karimzadeh, M. R. Ganjali, and A. Malekinezhad, Int. J. Electrochem. Sci. 12 (2017) 8033.
[72] T. Muthukumaran, S. S. Pati, L. H. Singh, A. C. de Oliveira, V. K. Garg, J. Philip, Appl. Nanosci. 8 (2018) 593.
[73] I. Karimzadeh, M. Aghazadeh, M. R. Ganjali, P. Norouzi, T. Doroudi, and P. H. Kolivand, Mater. Lett. 189 (2017) 290.
[74] M. Aghazadeh, and K. Yavari, Anal. Bioanal. Electrochem. 10 (2018) 1426.
[75] D. Sivakumar, M. M. Rafi, B. Sathyaseelan, K. M. Prem Nazeer, and A. M. Ayisha Begam, Int. J. Nano Dimens. 8 (2017) 257.
[76] X. Sun, C. Zheng, F. Zhang, Y. Yang, G. Wu, A. Yu, and N. Guan, J. Phys. Chem. C 113 (2009) 16002.
[77] W. Lu, Y. Shen, A. Xie, and W. Zhan, J. Phys. Chem. B 117 (2013) 3720.
[78] A. R. Bagherpour, F. Kashanian, S. A. Ebrahimi, and M. Habibi-Rezaei, Nanotechnol. 29 (2018) 075706.
[79] L. Lartigue, C. Innocenti, T. Kalaivani, A. Awwad, M. Sanchez Duque, et al., J. Am. Chem. Soc. 133 (2011) 10459.
[80] D. D. Herea, H. Chiriac, N. Lupua, M. Grigoras, G. Stoian, B. A. Stoica, and T. Petreus, Appl. Surf. Sci. 352 (2015) 117.
[81] H. M. Yang, H. J. Lee, K. S. Jang, C. W. Park, H. W. Yang, W. D. Heo, and J. D. Kim, J. Mater. Chem. 19 (2009) 4566.
[82] M. Aghazadeh, I. Karimzadeh, M. R. Ganjali, and M. Mohebi Morad, Mater. Lett. 196 (2017) 392.